

Impact of aerosols from the Asian Continent on the adjoining oceanic environments

K PARAMESWARAN*, SANDHYA K NAIR and K RAJEEV

Space Physics Laboratory, Vikram Sarabhai Space Centre, Thiruvananthapuram 695 022, India.

**e-mail: k_parameswaran@vssc.gov.in*

Aerosol optical depth (AOD) at 630 nm wavelength over the oceanic regions adjoining the Asian Continent is examined using a seven-year long data base derived from the Advanced Very High Resolution Radiometer (AVHRR) on board NOAA satellite to study the mean spatial and temporal variations as well as to understand the impact of aerosols advecting from the continent. Depending on the prevailing meteorological conditions and nature of synoptic circulation, the AOD over the oceanic region shows a systematic annual variation. This annual pattern in turn also shows an inter-annual variability because of the corresponding variations in the meteorological features over the continent as well as small-scale deviations in the nature of synoptic circulation. The annual variation over the oceanic regions also shows a pronounced spatial heterogeneity depending on the influence of continental aerosols. Making use of the wind speed dependence of sea-salt AOD at far-oceanic environments and monthly mean wind speeds at small grids of size $5^\circ \times 5^\circ$, the annual variation of sea-salt AOD at different locations is studied to understand the spatial heterogeneity of this component. The residual component obtained by subtracting this from the measured AOD is the non-oceanic component due to advection from continent. The source regions for major continental advectations are delineated from the analysis of air-mass back trajectories at appropriate locations identified from the annual pattern of non-oceanic component. The long-term effect of the continental impact is examined from the mean trend of AOD over the three major oceanic regions. This study shows that the continental influence is most significant over the Arabian Sea, followed by the Bay of Bengal and is almost insignificant in most of the regions over the Southern Hemispheric Indian Ocean, except for the effect of smoke aerosols over a few locations near Indonesia and Madagascar.

1. Introduction

Aerosol particles are mostly produced at the Earth's surface through various natural and anthropogenic processes. They get dispersed horizontally and vertically through prevailing circulation. Due to heterogeneity in sources, the aerosol properties vary from place to place. Oceanic environment is considered to be relatively pristine because the main source of aerosols in this region is the sea-salt produced through breaking of waves. The Gas to Particle conversion of Di-Methyl Sulphide (DMS) originating from phytoplankton

is also considered as a source of (non-sea-salt) aerosols over the ocean. However, as the source strength for these processes are mainly governed by synoptic meteorology, the spatial variation of the physical and chemical properties of aerosols including their concentrations over the oceanic region is expected to show a systematic variation with season which will be fairly steady from year to year forming a background aerosol system over the ocean. While the anthropogenic activity and prevailing meteorological conditions significantly influence the aerosol properties over the continent both directly and indirectly, wind speed is the

Keywords. Atmospheric Sciences; aerosols; remote sensing.

only prime parameter influencing the production of sea-salt aerosols over the ocean. Asia being a large and densely populated continent with rapidly expanding civilization, the increase in human activities can lead to increased production of aerosols. In addition to this, the meteorological condition prevailing over the continent, and its year-to-year variations can significantly influence the spatial distribution of aerosols. As the atmospheric circulation is not confined to the continental boundaries there will be an intrusion of aerosols from the continent into the oceanic environment. The proximity of inhabited continents could significantly alter the pristine nature of oceanic environment. The exact nature of this continental contamination/pollution in oceanic environment depends not only on the aerosol source strength over the continent but also the nature of synoptic circulation. Though the penetration of oceanic aerosols over to the continent is possible mainly through sea-breeze cells, its influence in general, is confined to few tens to around 100 or 200 kilometres from the coast depending on the topography and mesoscale features of the prevailing circulation because of their low concentrations and life times. The penetration of continental aerosols (especially the smaller ones) into the oceanic environment could be far deep because of the influence of synoptic circulation. Due to the increase in anthropogenic activity the impact of continental aerosols over the oceanic region becomes more and more significant with time. It may also be noted in this context that the aerosol impact on weather and climate, which is mostly regional in nature because of low residence time of tropospheric aerosols, strongly depends on the regional distribution of aerosol optical depth (AOD). Intrusion of continental aerosols over to the oceanic environment can modify the prevailing spatial distribution of AOD, which in turn can influence the spatial pattern of radiative forcing and thereby becoming an important factor in climate models.

The impact of aerosols from the Asian Continent over the adjacent oceanic region becomes important in this context. Satellite-borne measurements prove to be highly useful for this study because only this technique can provide the required information over such a vast geographical region with reasonably good spatial and temporal resolution. A reasonably long database of AOD derived from NOAA-AVHRR is used for this investigation. The main objective of the present study is to quantify the magnitude and regional extent of continental influence in these oceanic regions by examining the spatial variation of the mean annual AOD with due apportionment for the *in situ* generated sea-salt aerosols over the ocean by surface winds.

2. Data and analysis

Aerosol optical depths in the oceanic environment over the latitude region 25°S to 25°N between 40°E and 100°E derived from the upwelling radiance measured in Channel 1 of NOAA-AVHRR sensor at 630 ± 50 nm wavelength during the period November 1995 to December 2003 are used for the present investigation. This geographical zone covers the entire oceanic regions adjoining the south Asian continent, the aerosol advection over which is the main theme of this study. As the features of this data and method of deriving AOD are detailed in earlier publications (Rajeev *et al* 2000; Nair *et al* 2003, 2005) it is not elaborated here. The data from NOAA-14 is used for the period November 1995 to December 1999. After this due to the delay in its equatorial crossing time, the solar zenith angle for most of the pixels in the anti-solar side of the scan used for the retrieval of AOD became very high introducing large errors in the derived AOD values. Because of this, no AOD retrieval was attempted from NOAA-14 AVHRR data after December 1999. The data from the next satellite of the series, NOAA-16, became available only from March 2001, which resulted in a data-gap of 14 months. Variation of sea-surface reflectance with wind-speed is accounted using the Cox and Munk (1954) model. The AOD data from clear sky pixels identified employing appropriate cloud screening (Rajeev and Ramanathan 2001) only are used for the study. The AOD values thus obtained for each pixel with a spatial resolution of ~ 5 km at nadir (in Global Area Coverage format) form the basic data which is further grouped and averaged at appropriate grids and time-scales for studying different aspects.

The AOD values for each pixel derived from Level 1b AVHRR data are grouped in grid size of $1^\circ \times 1^\circ$ (in latitude and longitude) for all passes in each month and averaged over the study region. This grouping not only fills up the data gap, if any, but also smoothes them to a certain extent but reduces the basic spatial resolution to 100×100 km. This resolution is sufficient to study large-scale features in the spatial distribution (and seek their sources) that could perturb the atmospheric radiative forcing on a regional scale and thereby influencing the weather/climate system on a regional scale. However, as we will be dealing only with synoptic scale features of the mean circulation system influencing the AOD distribution as well as large scale transport of aerosols and not the small scale perturbations (in AOD) leading to environmental pollution near the coast, this coarse resolution is quite sufficient to achieve the desired objectives. The mean AOD in each grid is derived only when the number of clear sky days in

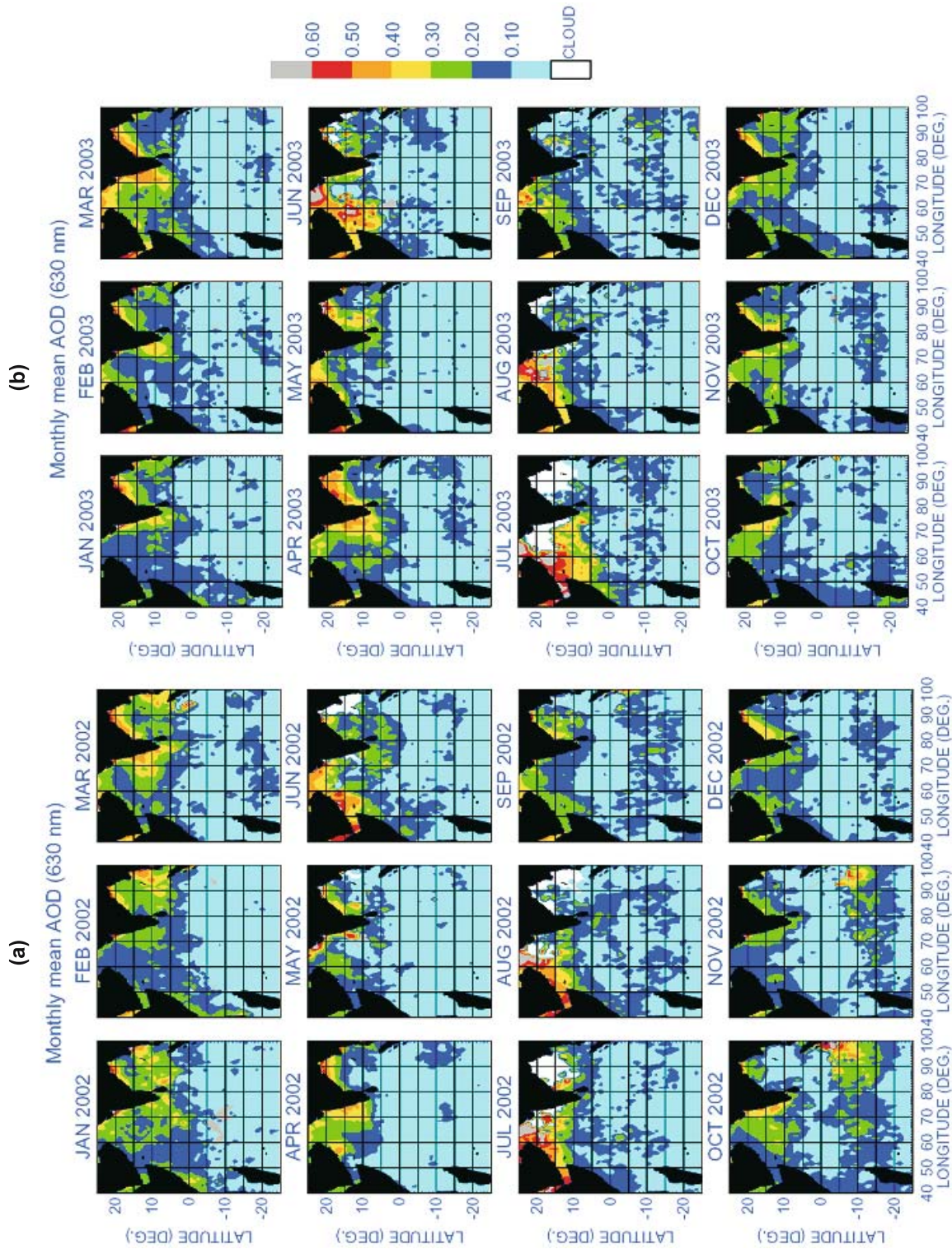


Figure 1. Map showing the spatial variations of mean AOD in different months over the oceanic regions adjoining the Asian Continent for two consecutive years 2002 and 2003.

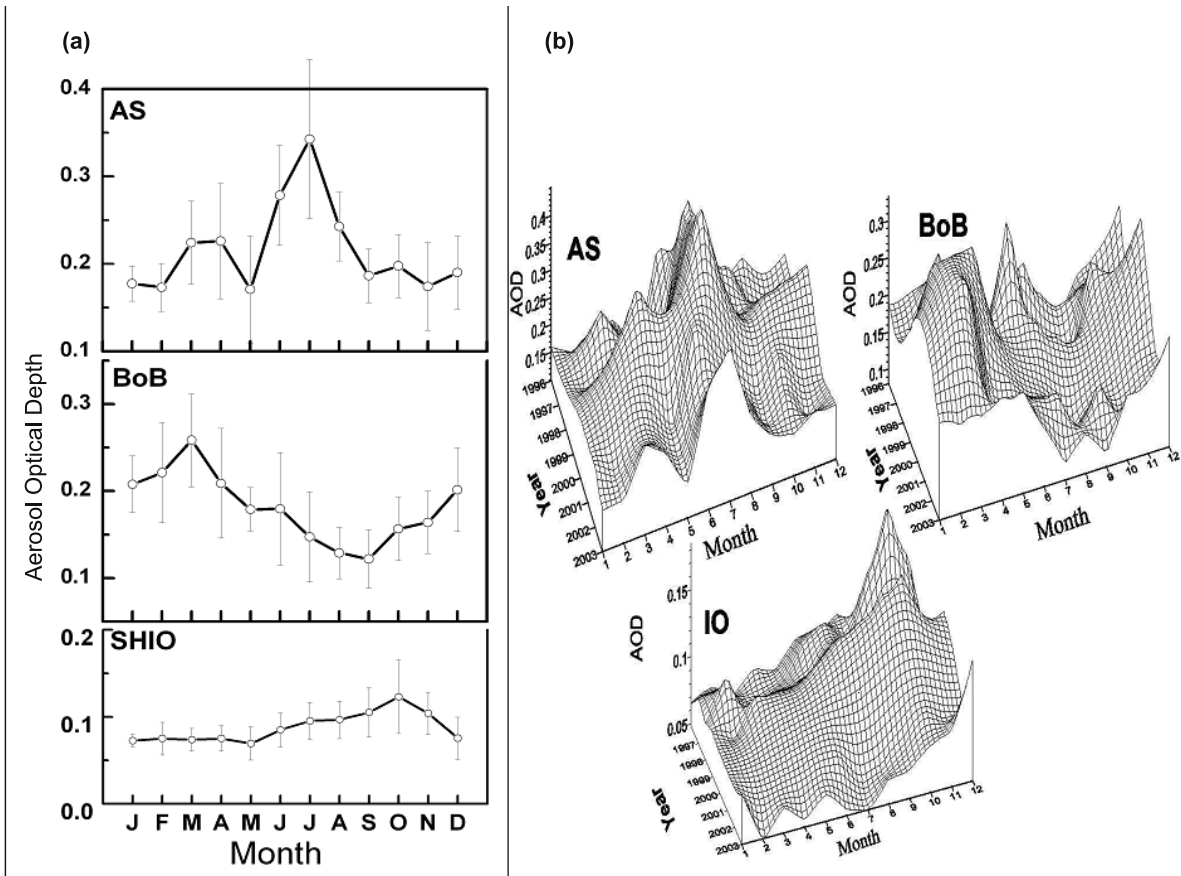


Figure 2. Mean annual variations of AOD over the three major oceanic regions adjoining the Asian Continent (a). Mesh diagrams showing the inter-annual variations in the mean annual patterns of AOD (for the period 1996–2003) over the Arabian Sea, Bay of Bengal and Indian Ocean (b).

a month exceeds three, which otherwise is marked as cloudy. Such data grids generated for each month in different years for the period of study are used to generate the monthly mean AOD maps for different years. The gross features in these maps remain more or less the same indicating that the pattern repeats from year-to-year. A noticeable deviation in the pattern is observed over the Southern Hemispheric Indian Ocean during the El Niño years. As a typical case, the mean AOD maps in different months for the two consecutive years 2002 and 2003 are depicted in figure 1; the former being a moderate El Niño year and the latter, a non-El Niño year. The colour codes indicating the AOD values are depicted on the right side of each figure. No AOD retrieval could be made in those regions, which are marked white in the figure because of cloudiness.

3. Results and discussion

A perusal of AOD maps in different years during the study period showed that in January the monthly mean AOD near the continental regions

in the Northern Hemisphere were generally less than 0.3. Except for some individual pockets of high AOD (with magnitude ~ 0.4), the highest AOD values over Arabian Sea and Bay of Bengal region generally lies around 0.3 during this month. The AOD in the Northern Hemispheric oceanic region increases moderately during the March–April period. Over the Arabian Sea it decreases significantly in May followed by a steep enhancement in June. It exceeds 0.5 over the western Arabian Sea with maximum values near the Arabian coast and decreasing towards east. This is true for all the years in the study period. The peak AOD and the area covered by AOD exceeding 0.3 increase from June and reach its maximum in July. The aerosol plume originating from coastal Arabia expands to cover the entire Arabian Sea by July. In July as the Head Bay of Bengal (HBoB) and north Arabian Sea regions are mostly cloudy in almost all the years, no systematic AOD retrieval could be possible for this region. But in certain years (e.g., 1999) some cloud free days were available making it possible to retrieve the AOD in this region. In these years the AOD values near the HBoB were less than 0.3. On an average, the

AOD values over the BoB were lower than those over the Arabian Sea even though it exceeds 0.2 in the western parts near the east coast of the Indian Peninsula.

An intense aerosol plume is seen near the equator (5°S to 15°S) during the September–November period of 1997 and 2002, extending from 70°E to 100°E in longitude with a very limited latitudinal width (less than about 10°). The plume observed in 1997 is significantly stronger (high AOD values over a large region) than that during 2002. In both these years, the plume starts in September, maximises in October and decreases from November to become almost insignificant by December. A pocket of high aerosol loading is also observed near the northwest coast of Madagascar during the November–December period (particularly during 1996 and 1998).

3.1 Annual variation of mean AOD over the oceanic regions

The mean AOD in each month for different years during the period 1996–2003 over the three major oceanic regions, Arabian Sea (5°N to 25°N , 45°E to 77°E), Bay of Bengal (5°N to 22°N , 80°E to 100°E), and Southern Hemisphere Indian Ocean (0 to 25°S , 40°E to 100°E), are estimated to study its mean annual pattern and the inter-annual variability. The northern boundary of 5°N for the Arabian Sea (AS) and Bay of Bengal (BoB) is selected taking into account the latitudinal extent of continental plumes observed in the Northern Hemisphere (figure 1). The region between 5°N and the equator (which is not included in any of the three sectors) is considered as a depletion region sandwiched between the northern hemispheric high and southern hemispheric low in AOD, the thickness of which is expected to vary with the strength of synoptic flow from the Northern Hemisphere.

The mean annual patterns of AOD in these oceanic regions are obtained by plotting the mean values in each month averaged for the entire period 1996–2003 which is presented in figure 2(a). Vertical bars in this figure indicate the associated standard deviations in different months. Over AS, the regional mean AOD is maximum in July (~ 0.34) and minimum (~ 0.17) in November. A secondary maximum is also observed in the March to April period (~ 0.22). Large standard deviations during the March to July period, when the mean AOD is relatively large, are mainly due to large spatial gradients and the inter-annual variability. Over the BoB, the mean AOD is large during the November–April period. The peak AOD with a magnitude of ~ 0.26 is observed in March. Minimum AOD in this region is encountered during the August–September period. Large standard

deviations associated with the monthly mean AOD in most of the months, except for August, is indicative of large spatial heterogeneity. The annual variation over the Indian Ocean is almost insignificant. Attributing these observed enhancements in AOD to continental aerosols it would be interesting to examine the possible sources responsible for these effects. In the Arabian Sea sector two prominent peaks are observable in figure 2(a) during March–April and June–August periods and correspondingly a prominent aerosol plume near the west coast of Indian Peninsula in March–April and another intense plume near the east coast of Arabia during June–August are observable in figure 1. In the BoB sector, a significant enhancement in AOD is observed in figure 2(a) during the December to April period with a peak in March and during this period the aerosol plumes near the east coast of Peninsular India and Head BoB are prominently seen in figure 1. In addition to this, an intense plume with lesser geographical extent is duly observable near the Myanmar coast during the January–April period. The area encompassed by these two plumes reaches a maximum in March. Over the Indian Ocean a weak enhancement in AOD is observed during October, which could be attributed to plumes emanating from peat (Levine 1999; Page *et al* 2002; Cochrane 2003) and forest fires over Indonesia during the El Niño years (Parameswaran *et al* 2004) to elevate the mean AOD over the SHIO.

The oceanic measurements carried out during the Indian Ocean Experiment (INDOEX), Arabian Sea Monsoon Experiment (ARMEX) and various other cruises have also shown high AOD over the Arabian Sea during the dry months (Satheesh and Moorthy 1997; Jayaraman *et al* 1998; Satheesh *et al* 1998; Kamra *et al* 2001; Prabha *et al* 2004; Moorthy *et al* 1998, 2005) and in June (Vinoj and Satheesh 2003). A positive gradient in AOD north of $\sim 10^{\circ}\text{N}$ over the Arabian Sea was also observed during these ship-borne measurements (Satheesh *et al* 1998; Jayaraman *et al* 2001; Moorthy *et al* 2001; Ramanathan *et al* 2001; Ramachandran 2004).

Though the gross features of tropospheric circulation remain more-or-less similar in different years, on finer scales their features do vary from year-to-year. These small changes influence the aerosol production, loss and transport notwithstanding the anthropogenic influences. Because of this, the annual AOD pattern over those oceanic regions that are under the influence of continental advection would show significant inter-annual variability. Figure 2(b) shows a mesh diagram depicting the annual variations of AOD in different years over AS, BoB and SHIO, the mean patterns of which are presented in figure 2(a). In the Arabian

Sea sector, the March/April peak in AOD, which was small in the initial years, showed an anomalous build up in 1999. After 1999, the amplitude of this peak shows a decreasing trend up to 2002. The high AOD during the summer monsoon period is very prominent in all the years from 1996 to 1999. In general, a similar pattern is observable for the AODs during the Asian dry period also. Over the BoB even though no sharp peaks are observable in the annual variation of AOD a broad peak is observable during the Asian dry period. This peak, which was very prominent during the period 1996 to 1999, decreased in subsequent years. Large values of AOD over the BoB near the east coast of the Indian Peninsula were also reported from ship-borne measurements (Ramachandran 2005). Over the Southern Hemispheric Indian Ocean the AODs are generally low and there is a systematic annual variation with a high during the October/November period, well prominent in 1997, 1999 and 2002.

The annual pattern of AOD observed over the Arabian Sea in the present investigation matches fairly well with that reported by Husar *et al* (1997) based on NOAA-AVHRR data (operational product) during the period 1989 to 1992. The peak during June–August is well reproduced in both the analyses. The secondary peak observed during the Asian dry period is more pronounced in the present study. The annual variation of AOD over the BoB though matching well in both these cases during the Asian dry period, showed a deviation during the June–August period. The present study however shows a decrease in AOD from May to September, while the analysis by Husar *et al* (1997) indicated a high in AOD which continued to persist up to August. As will be seen in the later part of this paper, the annual variation of AOD north of 10°N over the BoB matches well with that reported by Husar *et al* (1997), while that in its south showed deviation. The observed difference in the annual pattern between the two analyses thus can be attributed to the southward extension of the geographical region considered in the present investigation and the low density of data near the HBoB. Over the Southern Hemispheric Indian Ocean (SHIO), the AOD values are generally small. Largest value of AOD (~ 0.12) encountered in this region during October is comparable to the lowest values of AOD observed over other sectors. The lowest value of AOD over the SHIO is ~ 0.07 . Generally low standard deviations in this region compared to the other sectors indicate that the spatio-temporal heterogeneity is relatively small. The mean AOD over SHIO peaks in October, which corresponds to the peak of dryness when peat fires are very common over Indonesia. This annual variation in mean AOD over the SHIO also

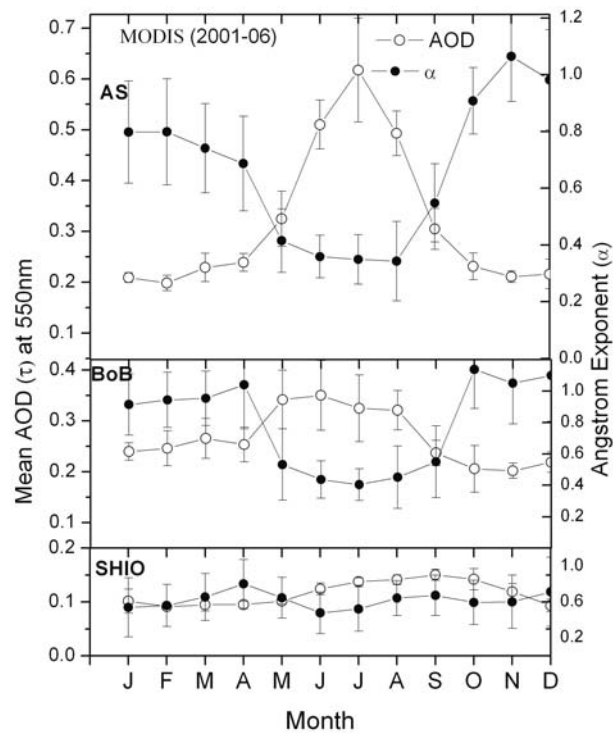


Figure 3. Annual variation of mean AOD at 550 nm over AS, BoB and SHIO from MODIS Terra, averaged for 1996–2003, along with the mean Angstrom exponent (α) for the year 2002 as a typical case.

matches fairly well with that reported by Husar *et al* (1997) for the Indonesian region, except for the fact that the October peak was more prominent in their case which again could be attributed to the difference in the geographical region considered in both these cases. While Husar *et al* (1997) considered only a small region near Indonesia for their studies, in the present analysis a larger geographical region covering the entire SHIO is considered.

In this context it would be worthwhile to examine the annual variation of AOD in these regions as measured by MODIS (Moderate Resolution Imaging Spectroradiometer), the data which is available from March 2000 onwards even though the wavelength of observation may not match with that of AVHRR. Monthly mean values of AOD at 550 nm obtained from their website for the period March 2000 to May 2006 are used to delineate the annual variation of AOD over the three oceanic regions described above. These are presented in figure 3. Along with the mean AOD the mean values of the Angstrom exponent (α) for the year 2002 (as a typical example) is also presented in this figure. A comparison of figure 3 with figure 2(a) shows that the amplitude of the summer peak over Arabian Sea is large in figure 3. It may also be noted that the standard deviations are also large during this period as seen in figure 2(a). Over the BoB the MODIS data show a

broad peak during the May–August period, which is not present in figure 2(a) (in which AOD shows a dip during July–September). The annual variation of AOD over SHIO is similar in both these figures. Adjusting for the wavelength difference using corresponding value of α it can be seen that the mean value of AOD reported from MODIS during the dry months over AS and BoB matches fairly with those derived from AVHRR, while the values of MODIS reported AOD during May–August period are larger. It should be noted in this context that we have applied a very stringent cloud screening procedure in processing the NOAA data (Rajeev and Ramanathan 2001; Nair *et al* 2004). This procedure effectively screens out all possible cloudy pixels as well as its adjacent ones based on spatial coherence test, which under any circumstances will not include the cloudy pixel, even if excludes a highly heterogeneous high AOD case. Nair *et al* (2004) have also demonstrated that this method is capable of distinguishing high AOD (dust episode) from cloud. During the southwest monsoon period the cloud cover over the HBoB is very large which could lead to relatively less number of clear sky pixels available for AOD retrieval. Then the mean curve presented in figure 2(a) could be more biased towards the southern parts of BOB. Additionally, it may also be noted that as reported by Zhang *et al* (2005) the MODIS values could be up to 20% overestimate when the frequency of occurrence of cloud is very large (as is the case over the AS and BoB during the southwest monsoon period) which also might have aided the observed difference.

3.2 Spatial variation in the annual AOD pattern over the oceanic regions

With the above background information on the month-to-month variation of mean AOD over the major oceanic regions surrounding the Indian subcontinent, the month-to-month variations of AOD at different locations over these regions are examined in detail to understand the continental influence in different parts of these major oceanic environments. The mean AOD over a grid size of $5^\circ \times 5^\circ$ over the Arabian Sea, Bay of Bengal and Indian Ocean have been selected and the month-to-month variations of AOD in these locations are examined in detail.

Figure 4(a) shows the month-to-month variations of mean AOD over these fine geographical grids in the Northern Hemispheric Arabian Sea and Bay of Bengal sectors. Because of the alignment of continents in these sectors, the number of grids decreases as one moves northwards from the equator. Even though the major features depicted in figure 2(a) for whole Arabian Sea sector between 5°N to 25°N , and 45°E to

77°E repeats in all, prominence of the peaks as well as the time of occurrences vary significantly. Almost all the curves for the Arabian Sea region in figure 4(a) show two distinct peaks in AOD, one around March–April period and other during June–July. While the April-peak is not very prominent in the two northern grids of the $20\text{--}25^\circ\text{N}$ sector, a well-defined peak with AOD exceeding 0.5 is observable in July. While the amplitude of July-peak decreases from north to south the amplitude of the AOD-peak in March/April increases near the Indian coast with a maximum in the $70^\circ\text{E}\text{--}75^\circ\text{E}$ sector. Studies carried out at Minicoy (8.3°N , 73.04°E) a tiny island in the Arabian Sea (Moorthy and Satheesh 2001) has also revealed the influence of mineral dust during winter when the winds are north-westerly (from west Asia). Cruise measurements carried out during INDOEX in February–March also showed (Moorthy *et al* 2001) high values of AOD in the mid-Arabian Sea region compared to that over the Indian Ocean near the equator and south of it. The July-peak is well pronounced near the Arabian coast and decreases towards east, even though it is observable up to the west coast of the Indian Peninsula. While in the longitude sectors east of 65°E , this peak is seen only in July, west of this it becomes more pronounced. Another feature observed in this region is the appearance of a small peak in October.

Results from a similar analysis for the BoB region are presented on the right-hand side panel of figure 4(a). It may be noted that the overall pattern of AOD variation over BoB shows a maximum during March–April followed by a minimum in September. This gross feature is observable in all the frames for BoB presented in figure 4(a). In addition to this general feature, near the HBoB a prominent high in AOD is observed during the March–June period with a peak in March, which matches well with that reported for the *Bengal* region by Husar *et al* (1997). Cruise measurements by Satheesh *et al* (2001) showed that in March the value of AOD (when adjusted to 630 nm) over the BoB near the Indian (off Chennai) coast ($\sim 82^\circ\text{E}$) is ~ 0.3 which decreases to < 0.2 over the Indian Ocean along the tip of Indian Peninsula (at 75°E near the equator) and increases back to > 0.4 over the eastern Arabian Sea. After June, AOD decreases significantly reaching its lowest value in September. The amplitude of the annual cycle, however, decreases significantly south of this latitude. South of 15°N a small peak observed in AOD during July is well pronounced over the mid-BOB region. This could be due to *in situ* production of sea spray. But the July-peak seen in $0\text{--}5^\circ\text{N}$ sector is due to aerosol advection from west (will be seen later in figure 6(a)). Another notable feature in the $0\text{--}5^\circ\text{N}$ latitude regions is the high

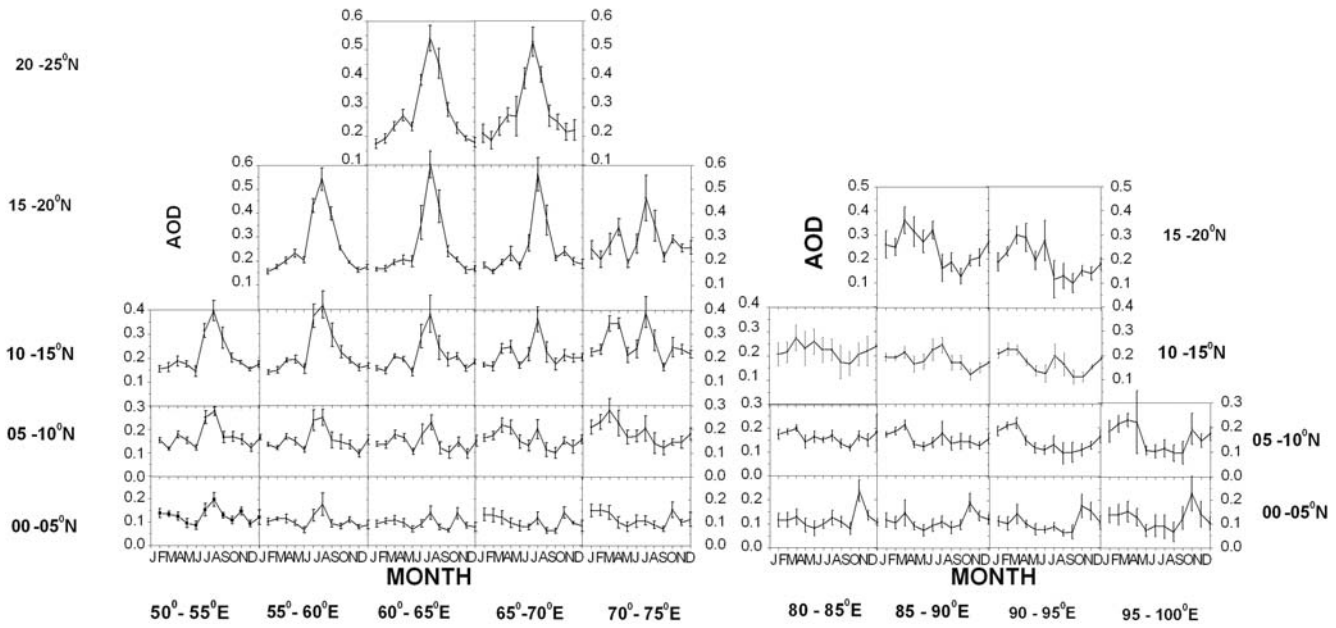


Figure 4(a). The mean annual pattern for AOD at different locations over the oceanic regions north of equator up to 25°N in the longitude region 40°E to 100°E at fine grid size of $5^\circ \times 5^\circ$. Vertical bars show the standard deviations.

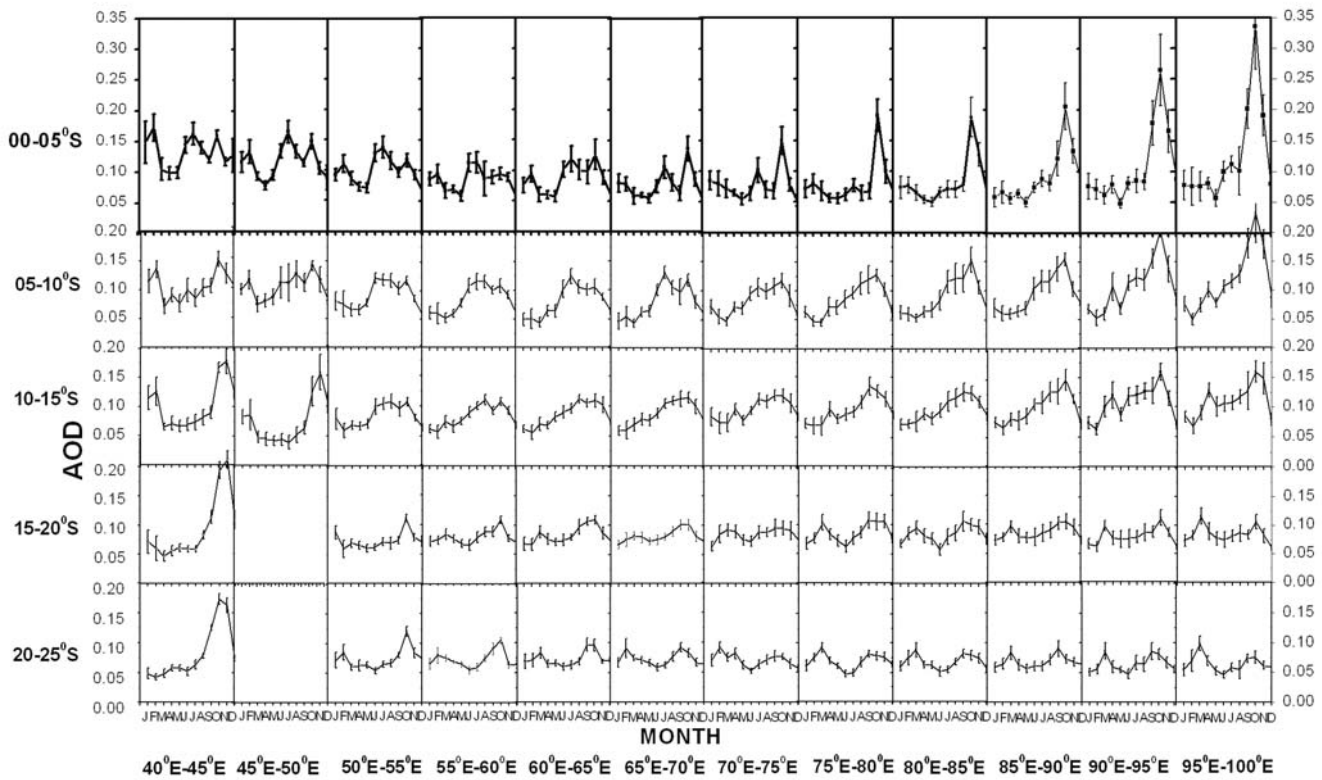


Figure 4(b). Same as figure 4(a) but for the oceanic regions south of equator up to 25°S.

in AOD appearing during October, the amplitude of which decreases from east to west (as will be seen later, this could be due to aerosol transport from the Indonesian region). An important feature observed is the decrease in the amplitude in the

March–April peak towards south near the Indian coast, while it continues to remain significant in the eastern coast of BoB all through the latitude region 0–20°N. In the mid BoB region, maximum AOD is observed in the March–April period and

minimum during September. Trajectory analysis for one full year presented in connection with studies on carbonaceous aerosols at Port Blair (11.7°N, 92.7°E), which will be true for the mid-BoB also, shows that air-mass reaching this location during November to April (dry period) originate from the Indian mainland and east Asian regions while those during the May–October period arrive from south western region of tropical Indian Ocean (Moorthy and Babu 2006). While the former set could carry continental aerosols from the regions where they originate, the latter should be more pristine in nature. This shows that the major aerosol advection over the BoB is from the northwest and northeast continents during the Asian dry period. This also favours a low AOD over mid-BoB during the southwest monsoon period (as observed), barring the local production.

The SHIO covers a large oceanic region extending in longitude from 40°E to 100°E covering a latitude region of 0 to 25°S in the present study. This region is relatively pristine with low AOD values compared to the Northern Hemisphere. The month-to-month variation of mean AOD in each of the 5° × 5° grids over the SHIO are presented in figure 4(b). Note that the spatial variation also is small in this region except for a few pockets of high AOD. In general, three distinct peaks, one each during January to February, June to September and October to November periods are observable in AOD. However, the prominences of these peaks vary with longitude and in some sectors one or two of these peaks become insignificant. In the latitude region 0–5°S, though all the three AOD peaks are distinctly seen in all the longitude sectors their amplitudes vary significantly. While both the January–February and June–September peaks are prominent in the western part, the October peak dominates in the eastern part. In the 5–10°S, the October peak is prominent in the western part while the June–September peak is prominent in the central part. In the first two longitude grids 40°E–45°E and 45°E–50°E, a prominent high in AOD is observed during the October to February period. Even though this feature extends up to 25°S, the width of this peak decreases and gets confined to the October–November period.

3.3 Sea-salt AOD over the ocean

In the pristine oceanic environment the aerosol concentration and hence the AOD depends mainly on two factors; one the gas to particle conversion of DMS originating from phytoplankton activity (Turner *et al* 1988; Leck *et al* 1990) and the other direct production of sea-salt aerosols (Blanchard and Woodcock 1957; Woodcock 1953; Monahan *et al* 1982; Smith *et al* 1989, 1993; Fitzgerald 1991;

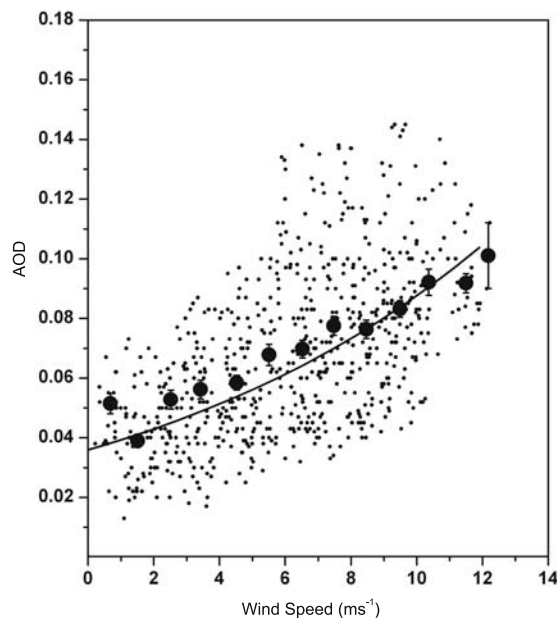


Figure 5. A scatter plot showing the variation of AOD with wind speed over relatively pristine oceanic environment over the southern hemispheric Indian Ocean. The solid circles present the mean AOD averaged at wind speed intervals of 1 ms⁻¹ with vertical bars indicating the standard error. The best fit mean curve for the scatter plot is also shown.

Wu 1993) from the sea surface through the interaction with surface wind. Agitation of sea surface by wind causes formation of bubbles, which subsequently break leading to the generation of aerosols. As the wind speed exceeds 3–4 ms⁻¹ white caps starts appearing over the sea surface (Monahan 1971), which further leads to the generation of more aerosols with a rate, which increases non-linearly with wind speed. Exton *et al* (1985) reported a non-linear increase in aerosol concentration in a marine environment with increase in surface wind speed especially when it exceeds 3 ms⁻¹. Several models are available in literature on the dependence of sea-salt concentration with surface wind speed (Erickson *et al* 1986; Gong *et al* 1997) most of which predict an exponential relationship between the two. However, significant difference exists between different models as far as the value of the coefficients are concerned. This is mainly due to the fact that the influence of wind on sea-salt properties over the ocean is rather complex. Aerosol size spectrum, which is fairly sharp at low wind speed, broadens with increase in wind speed (Fitzgerald 1991). Even though the aerosols generated by wind depends on the real time wind speed near the surface, their concentration also depends on the past wind speed because of their finite residence time. Thus, the role of wind in governing the sea-salt concentration over the ocean, which depends on local wind speed as well as the wind speed history, is very complex (Gathman 1983).

Additionally, the wind that is responsible for the generation of aerosols also plays an important role in their transport as well as deposition back to the ocean surface (Prabha *et al* 2005).

Most of the earlier works based on aerosol mass/number concentration (Lovett 1978; Hoppel *et al* 1990; Parameswaran *et al* 1995) showed that the concentration increases almost exponentially with wind speed with an index 0.16 m^{-1} as stated above. This increase in aerosol concentration mainly in the marine boundary layer can enhance the AOD. Based on long-term measurements carried out at Minicoy Island in the Arabian Sea, Moorthy and Satheesh (2000) reported a value between 0.05 and 0.11 for the exponential index in the spectral range $0.38\text{--}0.9 \mu\text{m}$. Cruise measurements carried out over the Arabian Sea and Indian Ocean (Moorthy *et al* 1997) also yield a value in the range of 0.07 to 0.13 for the index. Based on these reports a value of 0.08 for the index is found to be sufficiently accurate for the wavelength band used in the present study. However, we have also examined the wind speed dependence of AOD over far oceanic regions using the AVHRR derived AOD along with the corresponding surface wind speeds from NCEP/NCAR reanalysis (at 1000-hpa level). Though the change in sea surface reflectance due to wind will influence the retrieved values of AOD from satellite-measured radiance, this effect is taken into account using the Cox and Munk (1954) model as stated in section 2. Note that, here we use the monthly mean AOD and wind speed both averaged for a grid size of 2.5° for the present study mainly because of the fact that no real time collocated measurements could be available from the data source. A geographical region bound between $5\text{--}25^\circ\text{S}$ in the longitude region and $50\text{--}80^\circ\text{E}$ for the year 2003 is selected for this study. A scatter plot of the 1000-hpa-wind speed and AOD generated using this data is presented in figure 5. A clear non-linear increase in AOD with increase in U was observable even though with some scatter. In order to smooth out this scatter the AOD values at wind speed intervals of 1 m s^{-1} are averaged. The mean values are presented in this figure with vertical lines representing the associated standard error. An exponential relation of the form $\tau_{\text{ss}} = \tau_{\text{ss0}} \exp(bU)$ is established between the sea-salt AOD (τ_{ss}) and U . The coefficient τ_{ss0} represent the AOD for zero wind speed and b is the exponential index. The best-fit value of τ_{ss0} is 0.04 ± 0.001 and that of b is 0.08 ± 0.03 which is fairly in good agreement with those reported from real time *in situ* measurements of wind speed and AOD considering the uncertainties associated with the parameters. Note that, the value of τ_{ss} estimated in the present study based on coefficients derived from mean values also compares favourably (within its uncertainty limits)

with those estimated through the empirical relations evolved from real time collocated measurements cited above.

3.4 Non-sea-salt component and continental influence

Over the oceanic regions relatively close to the continent, the intrusion of continental aerosols will be significant. The observed AOD in these regions could be much larger than that due to the sea-salt aerosols. The contribution of continental advection on the measured AOD in such cases can be estimated by subtracting τ_{ss} from the measured aerosol optical depth (τ), which we refer to hereinafter as τ_c . It should be noted in this context that the sea-salt component estimated using the above method provides a mean trend for the wind speed dependence and the best-fit curve represented by the established relationship is fixed through the middle portion of the scatter plot having a significant number of points falling below this mean line for which the computed wind contribution will be more than the actual measured τ . In such cases the estimated τ_c will be negative (which is physically meaningless). So any mean value of τ_c falling below zero is treated as zero for our further discussion (insignificant continental contribution). Similarly considering those points which lie above the mean line in this scatter plot of τ and U , there will be an underestimate of τ_{ss} . Because of the uncertainties associated with the coefficients (especially, b) the estimated τ_{ss} will have an uncertainty (standard error) of -20% to $+30\%$ for a moderate wind speed of 10 m s^{-1} , which increases with the increase in wind speed. The uncertainty in τ_c thus depends mainly in the accuracy with which τ_{ss} is estimated. Considering, these factors, any small value of τ_c within the standard deviation of τ_{ss} estimated using the above relationship, is treated as insignificant.

Using the above relationship and the mean wind speed in different months over the oceanic region, the month-to-month variations of τ_{ss} at different locations are examined in detail. The month-to-month variation of τ_{ss} and τ_c thus obtained for different locations over the Arabian Sea and BoB are presented in figure 6(a). Similarly the mean annual variation of τ_{ss} and τ_c over the southern hemispheric part of the Indian Ocean at different geographical grids up to 25°S for the longitude region $40\text{--}100^\circ\text{E}$ are presented in figure 6(b). In order to facilitate a direct visual comparison of AOD values and its month-to-month variation in different grids, as far as possible the same ordinate scale is used in all frames in these figures. But, because the geographical variation of AOD over the SHIO is very large especially near Indonesia, a compressed

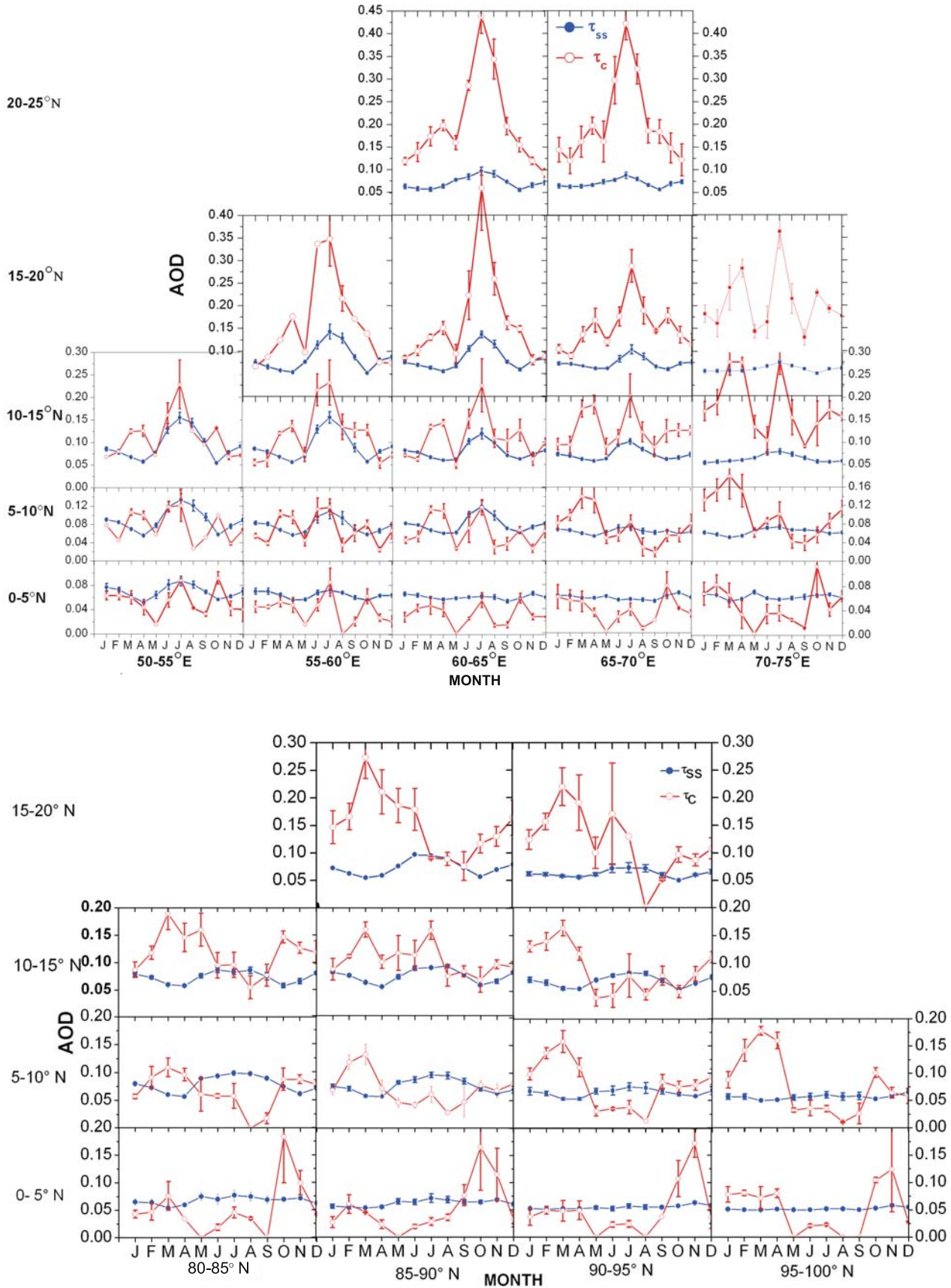


Figure 6(a). Annual variation of sea-salt and non-sea-salt component of AOD at different locations over the oceanic region north of equator in the longitude region 50°E to 75°E (Arabian Sea part) in the top panel and 80°E to 100°E (Bay of Bengal part) in the bottom panel. Vertical bars indicate the respective standard deviations.

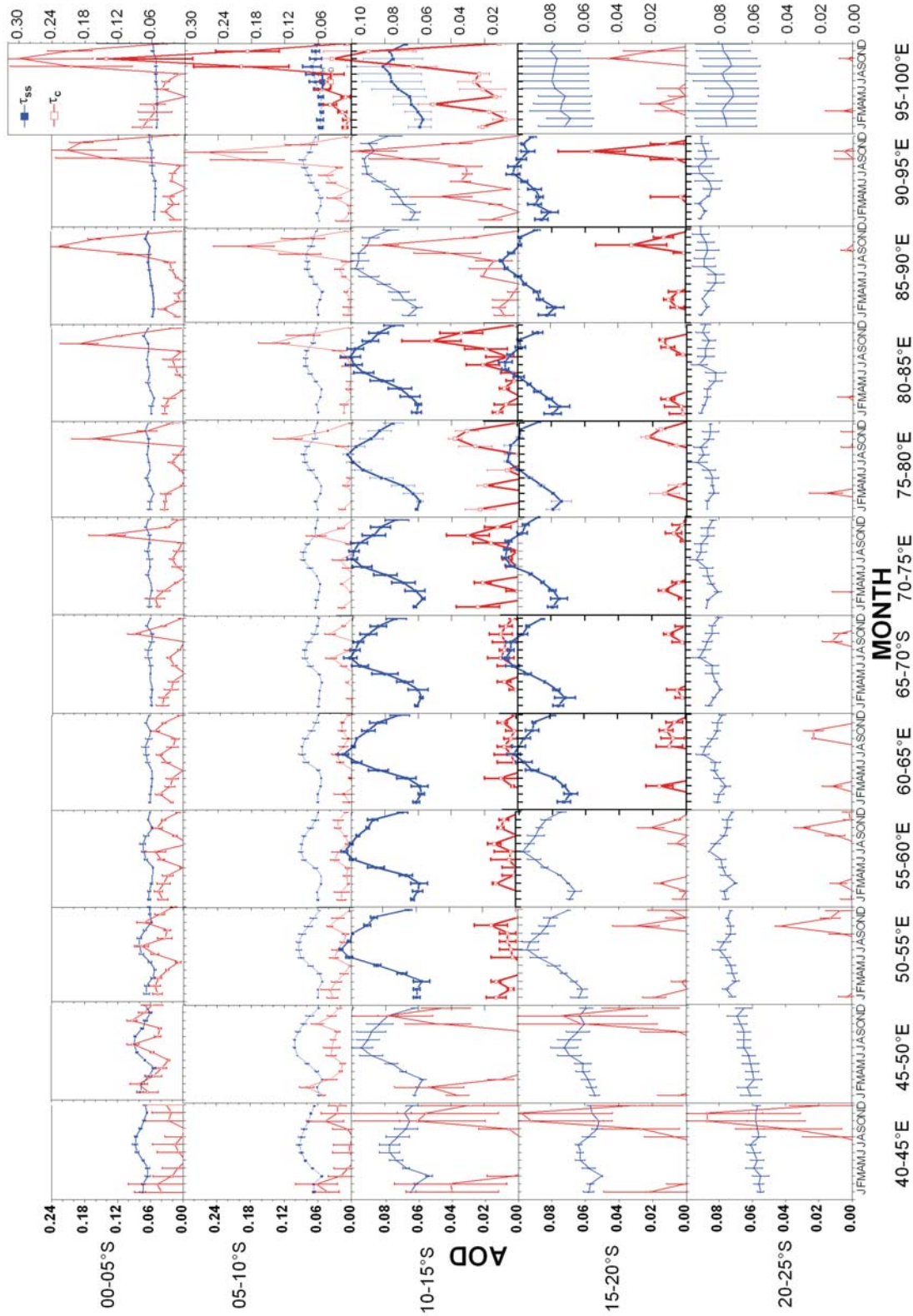


Figure 6(b). Annual variation of sea-salt and non-sea-salt component of AOD at different locations over the oceanic region south of equator in the longitude region 40°E to 100°E (southern hemispheric Indian Ocean). Vertical bars indicate the respective standard deviations.

ordinate scale is used for the two top rows in figure 6(b). However, invariably the same scale is used for all the frames along the same latitude sector. A perusal of figure 4 along with figure 6 clearly depicts the nature of continental impact over these oceanic regions. The deviation of AOD in each grid of figure 4 from the corresponding value of τ_{ss} in figure 6, the magnitude and nature of (annual) variation of which is represented by τ_c , is the contribution from the continents. Note that, AOD values used in this analysis are for 630 nm, which will be more sensitive to extinction due to particles in the ‘accumulation’ and ‘large’ size modes and less sensitive to that in the sub-micron mode. As the abundance of sub-micron particles will be quite significant in continental aerosols this influence would be more prominently desirable if the measurements were made on a shorter wavelength.

3.4.1 Arabian Sea

Over the Arabian Sea, τ_{ss} in general, shows a systematic semi-annual variation with a prominent peak around July and a relatively small secondary peak during the December–January period, with two minima in April and October respectively. This periodic variation in τ_{ss} that is very prominent in the western parts decreases steadily towards east and becomes almost insignificant near the west coast of the Indian Peninsula (70–75°E). Near to the equator (0–5°N region) this periodic variation in τ_{ss} becomes less prominent at east of 60°E. The values of τ_{ss} in general and the amplitude of July-peak in particular are the largest in the region 5–20°N and decreases on either side. In general, τ_c shows a prominent maximum in July and a secondary maximum during the March–April period. The July-peak in τ_c , which is very prominent and well-defined in the latitude region 20–25°N, decreases steadily in amplitude towards south. Similarly the amplitude of this peak is relatively large in the western parts of Arabian Sea and decreases towards east. Unlike the above, the secondary peak that is more prominent in the eastern parts of the Arabian Sea decreases towards west. This peak is well pronounced in the latitude region 5–10°N and decreases steadily in amplitude towards north and rather abruptly towards south. In this latitude region west of 65°E the amplitude of two peaks (April and July) are comparable and east of this the April-peak becomes more prominent. Another sharp peak in τ_c also starts appearing in October at the region south of 15°N, which becomes well pronounced in the latitude region 5–10°N in the western Arabian Sea. The variation of its amplitude suggests that it is contributed by an aerosol advection from west in the region 10–15°N and from both east and west in the region 0–5°N.

Note that the values of τ_c , which are significantly larger than τ_{ss} in the northern latitudes beyond 10°N, become comparable in latitudes south of 5°N. In the depletion region (0–5°N) τ_c is less than or comparable to τ_{ss} .

This analysis clearly shows that the continental intrusion over the Arabian Sea mostly comes through two regions; one from the east of 75°E, the influence of which is largest during the March–April period and the other from west of 60°E the influence of which is largest during the June to September period. While the former advection is more aligned towards south the latter is more aligned towards northwest. From the synoptic flow pattern (Nair *et al* 2005) and figure 1, it can be stated that the source of the former advection is centred around the Indian Peninsula ($\sim 10^\circ\text{N}$) and the latter on Arabia ($> 20^\circ\text{N}$). The influence of Arabian dust becomes almost insignificant near the equator (0–5°N) east of 65°E where the October peak becomes well-pronounced. This peak in τ_c is not very significant near the west coast of peninsular India but fairly prominent west of 70°E. It may also be noted that the April-peak becomes rather weak near the equator.

3.4.2 Bay of Bengal

In general, the values of τ_{ss} in different latitude belts over the BoB are slightly lower than the corresponding values over the Arabian Sea, even though the nature of variation is more or less similar to that over the Arabian Sea. In the northern latitudes beyond 5°N, τ_{ss} shows two broad peaks during the May–September and November–February periods. Minimum in τ_{ss} occurs around April and October. This annual pattern is more pronounced in the northern latitudes and less significant in the depletion region (0–5°N). Similarly, the amplitudes of the two peaks are largest in the western parts of the BoB (east coast of Indian subcontinent) and decreases towards east and becomes insignificant at east of 95°E at north of 5°N, and at all longitudes south of 5°N. The non-sea-salt component also shows two prominent maxima, which are shifted in time. The first maximum occurs during the March–May period and the second one during the October–December period. The amplitudes and widths of these two peaks are largest at 15–20°N and decreases towards south. At latitudes north of 10°N, τ_c in general and during the November–June period in particular is significantly larger than τ_{ss} . The annual variations of τ_{ss} and τ_c in these regions are opposite in phase. In the latitude region 5–15°N, the peak in τ_c during the January to March period is very prominent in the eastern part and decreases towards west. In general, τ_c is minimum during the summer

monsoon period and is comparable to the corresponding values of τ_{ss} notwithstanding the fact that τ_{ss} show a broad peak during this period. At $0-5^\circ\text{N}$, on an average, τ_c is less than τ_{ss} except for the sharp peak in τ_c appearing in October and the annual pattern shows a smooth transition from the Arabian Sea to BoB.

3.4.3 Southern Hemispheric Indian Ocean

Over the Southern Hemispheric Indian Ocean, the annual pattern of τ_{ss} and τ_c shows significant variation from one location to the other. The annual variation in τ_{ss} is small near the equator and becomes very prominent in the latitude region $5-15^\circ\text{S}$ and again decreases further south to become almost insignificant at south of 20°S . It shows a well-defined peak during the June–July period with a small secondary peak in January. On an average, except near the Indonesian region, which is strongly influenced by biomass burning during the September–November period (particularly observable east of 70°E between equator and 15°S), the values of τ_c are always less than those of τ_{ss} . Similarly a peak in τ_c is observed in the $40-45^\circ\text{E}$ sectors, south of 15°S , which could be again due to intrusion of continental aerosols possibly from the adjacent land mass. In the longitude sector north of 15°S a small peak in τ_c is observable during February also. A less pronounced continental influence is observable in all the longitude sectors up to 10°S even though the values of τ_c on an average are less than τ_{ss} . A similar feature is observable at all longitudes west of $\sim 50^\circ\text{E}$ and at $0-15^\circ\text{S}$ in the region east of 85°E . At other places τ_c is negligibly small and can be ignored considering the associated uncertainties. A general increase in the amplitude of the July-peak in τ_{ss} is observable from west to east in the latitude region 5°S to 20°S .

The region $90^\circ\text{E}-100^\circ\text{E}$ at $0-10^\circ\text{S}$ is close to Sumatra and Indonesia where forest and peat fires are very common during September to November. A similar condition exists during October–December near the $40^\circ\text{E}-50^\circ\text{E}$ sector in $10-25^\circ\text{S}$ latitude band, which is near to the African Continent. At these two oceanic sectors the major source of aerosols during October–November could be from the biomass burning over the adjoining continents. To make a more quantitative assessment of this, the monthly mean fire counts over the relevant continents are examined from ATSR world fire atlas. Figure 7 shows a plot of mean fire counts over South East Asia ($0-10^\circ\text{S}$; $100^\circ\text{E}-120^\circ\text{E}$) and South Africa ($10-25^\circ\text{S}$; $30^\circ\text{E}-40^\circ\text{E}$), which are adjacent to the above-referred grids. A good correspondence between fire counts and AOD is observable in these figures, which indicates that increased biomass burning over South East Asia and South African

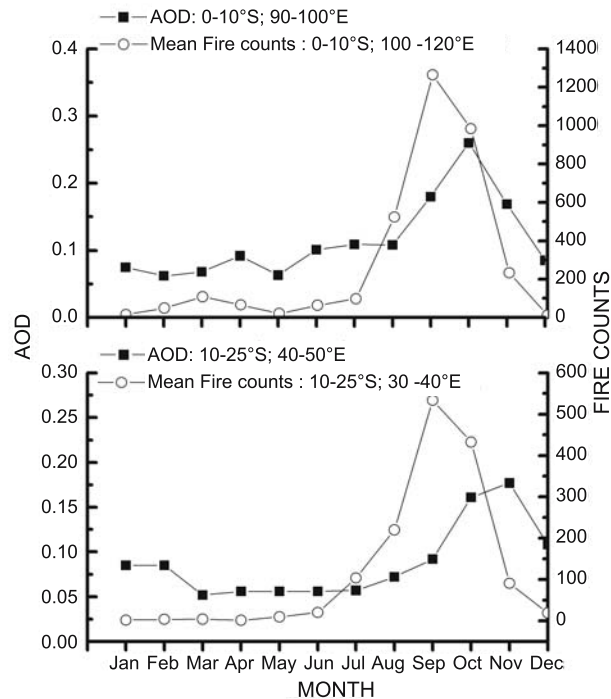


Figure 7. The AOD at two locations over the southern hemispheric Indian Ocean where its annual variation deviated significantly from that of wind alongwith fire counts derived from ATSR over the adjacent continental region.

regions significantly influence the annual pattern of AOD in the two respective zones adjacent to these two landmasses. As the intrusion of aerosols from different parts of the Asian Continent in the adjoining oceanic environments strongly depends on seasonally varying synoptic circulation, the effect is felt at different regions in different periods of the year. Even though the sources of these aerosols are more or less understandable from figures 1 and 6, to make a more quantitative assessment it is necessary to examine the air-mass characteristics associated with this transport. For this a few locations over these oceanic regions are selected based on figures 1 and 6.

3.5 Air-mass trajectories to identify the major sources

From figure 6 the regions at which and the periods in which a prominent peak is observed in τ_c are identified and correlating this with the AOD map in figure 1 the locations where the continental influence is pronounced are selected. Nine locations over these oceanic regions thus selected for this study are; 12°N , 70°E and 15°N , 60°E over the Arabian Sea, 18°N , 90°E ; 15°N , 97°E ; 10°N , 97°E and 2°N , 90°E over the Bay of Bengal and 5°S , 95°E ; 20°S , 42°E and 5°S , 42°E over the Southern Hemispheric (Indian) Ocean. Trajectories of air mass reaching these regions during the period when the

plume is very prominent are examined. These trajectories reaching at different altitudes over a particular location need not originate from the same region because the synoptic circulation at different altitudes during the same period of the year need not be similar (Nair *et al* 2005). As significant contribution of AOD comes from the lower troposphere below ~ 4 km, we have taken the air trajectories reaching at 1.5 km as representative of major aerosol advection responsible for the enhancement in AOD. In the lower troposphere above 1 km the average residence time of aerosols in the accumulation mode (which is mainly responsible for the observed AOD at 630 nm) is of the order of one week (Jaenicke 1984). Hence, a seven-day air trajectory was sought backwards from the region of interest to trace the source region. These air trajectories for different days are obtained from the NOAA-ARL-HYSPLIT transport dispersion model through a global reanalysis using archived data set (Draxler and Rolph 2003; Rolph 2003).

From figure 6(a) it can be seen that over the Arabian Sea major enhancement of τ_c occurs during the March–April and June–August periods. From figures 1 and 6 it can be seen that these high τ_c values are mainly contributed by the aerosol plume near the west coast of peninsular India during the former period and that near the east coast of Arabia during the latter period. Keeping this in mind all the daily seven-day air trajectories reaching at 12°N , 70°E at 1.5 km in March for the former case and those reaching at 15°N , 60°E at 1.5 km level in July for the latter case are traced for the year 2003 and presented in figure 8. For all the subsequent air trajectory analyses also we have taken the year 2003 as a typical case for this study. The location at which and the month in which the analysis is made is indicated at the top of each panel. The colour code used for indicating the altitude of air parcel at different locations during its course along a particular trajectory is presented in the respective frames. Similarly in the BoB sector (figure 6a) to delineate the source of aerosols reaching the HBoB (at 1.5 km), a location at 18°N , 90°E is selected and air mass trajectories are traced back in time for different days in March and presented in figure 8. There are two more locations identifiable in this sector where high values of τ_c are encountered. These are 15°N , 97°E near Myanmar coast and 10°N , 97°E near Thailand. Back-trajectories of air mass reaching at these locations in March are examined to delineate the sources responsible for this feature and are shown in figure 8.

On examining the trajectories ending near the west coast of peninsular India, a significant number of them originate from the Indian subcontinent either from the same level or above while

some of the trajectories originate from the west coast of peninsular India. A few trajectories originating/advection through the BoB along the east coast turn westwards to reach this location. The continental region that is responsible for the plume is clearly observable in this figure. Similarly in July most of the trajectories ending 15°N , 60°E originate from the arid-region of Arabia. They originate from a higher altitude and descend to 1.5 km while proceeding towards the observation point. These air parcels can transport abundant mineral dust from the arid region of Arabia over to the Arabian Sea. Our earlier studies (Nair *et al* 2005) also showed that at higher altitudes the air mass advection is mostly from Arabia while at lower altitudes they are from the oceanic region near Madagascar and coastal regions of Africa. But a detailed analysis of wind convergence at different altitudes in this region, however indicate that most of the aerosol transport occurs around 1.5 km.

On examining the air trajectories ending at 18°N , 90°E (figure 8) it can be seen that quite a few of these trajectories originate from the arid region of Arabia, Pakistan and pass through the north Indian plains to sink near the HBoB. Significant number of them also originate from the Gangetic plains. The length of these trajectories are quite large indicating the dominance of long-range transport. Quite a few trajectories that originate from the east coast of peninsular India also reach this point through an overturn occurring near the east coast. Following a similar procedure, the pattern of aerosol transport leading to the formation of a high AOD region near Myanmar is examined by analysing the air trajectories reaching at 15°N , 97°E in March. Figure 8 shows that most of these trajectories are from the southeast Asian region. Though quite a few trajectories originating from higher altitudes over the Indian subcontinent also reach this location, the aerosol content at such high altitudes could be too small to produce a significant impact. The trajectories ending at 10°N , 97°E also show that significant advection of continental air mass during March occurs from the southeast Asian region. This shows that the observed increase in τ_c (figure 6a) at this location should then be attributed to the advection of aerosol-laden air from the southeast Asian region. In the latitude sector 0 – 5°N , a well-defined high in τ_c (but comparable to τ_{ss}) is observable during the June–August period (with a peak in July). This is the remnant of mineral dust advection from Arabia, which becomes almost insignificant south of equator. This peak is more significant in the western longitudes and steadily decreases towards east and becomes almost insignificant over the BoB sector. In the same latitude sector another well-defined peak is observable in τ_c during October

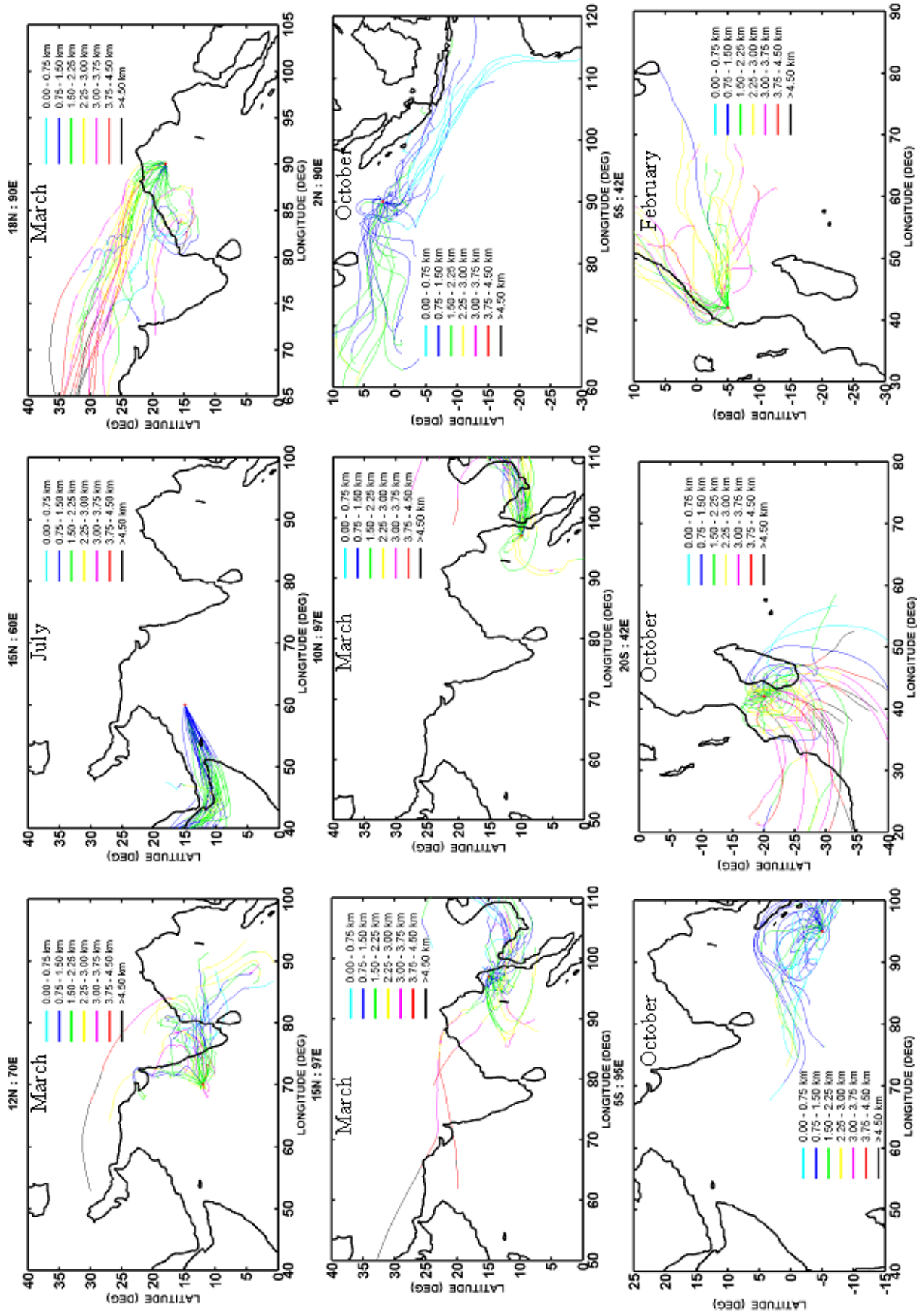


Figure 8. Air-mass back trajectories ending at a few selected locations over the Arabian Sea, Bay of Bengal and southern hemispheric Indian Ocean showing the relevant continental advection.

prominently in the BoB sector. In order to delineate the source of aerosols responsible for this feature air trajectories reaching at 2°S, 90°E are examined (figure 8). Even though a significant number of trajectories originate from the western parts, quite a few originating from the Indonesian coast also reach this location. The observed high in τ_c at this location could thus be due to the aerosol advection from the Indonesian side.

The source and pathways of aerosol transport leading to the formation of high AOD region over the Indian Ocean is examined by analysing the trajectories ending at the corresponding locations at relevant times. The back-trajectories for the four typical cases selected for this study are presented in the right-most panel of middle row and the base panels in figure 8. As can be seen from figure 6(b), a significantly large peak in τ_c is observed near Indonesia during October in the eastern part of the Indian Ocean around 5°S. To study the air-mass advection in this region, a location 5°S, 95°E is selected and all trajectories reaching at this location at 1.5 km are presented in figure 8, which shows the influence of the Indonesian subcontinent. Note that 2003 was a non-El Niño year and during the El Niño years the trajectories are better aligned to Indonesia. Similarly to examine the peak in τ_c during this period near Madagascar a location at 20°S, 42°E is selected. Most of these trajectories show air-mass advection from the African Continent as well as from Madagascar. As seen from figure 7, the AOD at this region during the relevant period showed a good correspondence with fire counts over the African Continent, which further confirm that the aerosols responsible for this high AOD originated from the African Continent. The fourth location selected over the Indian Ocean is around 5°S, 42°E during February. Figure 8 shows that part of the air-trajectories arriving at this location originate from the Northern Hemisphere. This indicates the existence of a cross-equatorial flow, which carries the northern hemispheric air from Arabia and Somalia into the Southern Hemisphere.

3.6 Trends in aerosol optical depth over the oceanic region

The present day concern is the increase in aerosol generation from the continental sources and its impact on regional and global climate. A significant component of these aerosols could be of anthropogenic origin. Systematic measurements carried out over the continent indicated a clear increasing trend in columnar AOD due to increased loading of aerosols in the past two decades (Parameswaran *et al* 1998; Moorthy *et al* 1999; Satheesh *et al* 2002). As the advection of

continental aerosols over to the oceanic region is quite significant in this region, a similar trend can be expected over the oceanic environment also. For assessing the magnitude of this trend in the oceanic environments the time series of mean AOD over the three major oceanic sectors are examined. As the amplitude of the annual variation is quite significant over these regions, in order to study the long-term trends the monthly mean AOD values are smoothed using an 11-month running mean window. These smoothed values of AOD over the three oceanic regions (AS, BOB, and SHIO) are presented in figure 9. The vertical bars indicate the weighted mean standard deviation (σ_τ) estimated

as $\sigma_\tau = (1/n)\sqrt{\sum_{i=1}^{i=n} \sigma_{\tau_i}^2}$; where n is the width of the running mean window and σ_{τ_i} is the standard deviation of the mean AOD (τ_i) in individual months. To avoid any artefact due to data gap during January 2000 to February 2001 the running mean is taken separately for the data before and after the gap confirming that in each running mean window at least 10 values are available. This increases the data gap in figure 9 to two years. The top panel in this figure shows the trend for AS, the middle panel that for BoB and base panel the same for SHIO. For comparison, a similar running mean of the corresponding AOD values at 550 nm from MODIS also is presented in respective frames. As MODIS data are available only from March 2000, the running mean is presented from August 2000 to December 2005. Because of the large amplitude of the annual peak in the AS sector, the running mean could not effectively smooth out this variation. The trend of AOD in both the cases (AVHRR and MODIS) for a particular region compares favourably for the overlapping period except for the difference in base level. The MODIS data show a small decreasing trend after 2003 in the AS sector. The AVHRR derived AOD in this sector shows an increasing trend up to the year 1999 followed by a small dip and then levelling off. This trend compares favourably well with that reported, based on measurement carried out over the continent (Satheesh *et al* 2002). Though a similar trend is observable over the BoB, also the magnitude of increase is relatively small compared to that in the AS sector. The mean value of AOD during 2001–2003 on an average is comparable to that during 1997–98 over the AS and BoB. It is highly likely that the high AOD of 1999 reported by various investigators (Rajeev and Ramanathan 2001; Jayaraman *et al* 2001; Moorthy *et al* 2001) and attributed to increased off-continent flow and increased subsidence by Nair *et al* (2003) has contributed significantly for this anomaly. However, the data gap during 2000 prevents a more detailed explanation for this episode. No significant

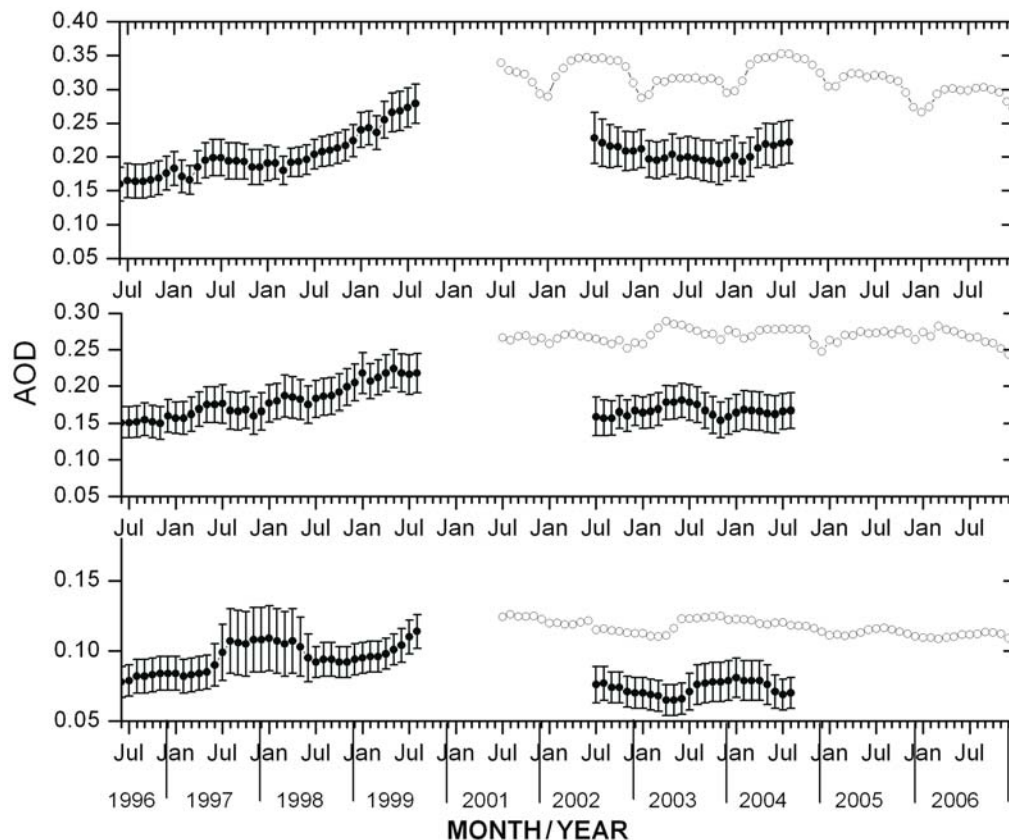


Figure 9. Plots showing the variation of smoothed AOD derived from AVHRR at 630 nm (solid dot with vertical bar) along with that of MODIS-reported AOD (operational product) at 550 nm obtained from website, using an eleven-month running mean window, over the three major oceanic environments depicting the long-term trends.

increasing trend in AOD is observable over the SHIO. A small dip after 2001 could be attributed to the influence of the major smoke episode over Indonesia adjoining oceanic environment in 1997 and the resulting elevation of mean AOD in this region during the period before 2000 (because of the effect of running-mean smoothing). The mean level observed after 2001 could be the background base level of AOD prevailing over SHIO.

4. Conclusion

Based on the above analysis it can be concluded that the impact of aerosols from the Asian Continent over to the oceanic region of Arabian Sea, Bay of Bengal and Indian Ocean is significant. This influence is prominently seen over the Arabian Sea followed by the BoB. The continental impact is minimum over the Indian Ocean in general, even though the influence of the Indonesian plume in the eastern parts is significant during the September–November period. The continental advection is well-pronounced in different parts of the oceanic region at different periods. Because of this the annual pattern of AOD over the oceanic regions significantly differs from the annual pattern

of synoptic wind speed (or equivalently the annual pattern of sea-salt AOD). The sea-salt AOD shows a pronounced annual variation in the latitude region 5–20° (with maximum amplitude at ~15° latitude) on either side of the equator, while its annual variation is almost insignificant near the equator and beyond 20°. Depending on prevailing wind speed the mean value of this component varies from 0.04 to ~0.12.

Over the Arabian Sea, the significant impact of continental aerosols is observed during the March–April period from the Indian subcontinent and during the June–September period from the Arabian deserts. Similarly over the BoB the influence of Indian subcontinent is significantly felt during the November–May period. Significant continental influence is observed in the eastern parts of BOB south of 10°N during the same period also, which steadily decreases towards west reaching a minimum near the east coast of peninsular India. During the June–September period the BoB region is relatively pristine with a minimal influence from continental aerosols. The sea-salt AOD during this period is comparable to the non-sea-salt component. In both these oceanic regions (AS and BoB) the continental influence is highly significant in the

northern parts especially north of $\sim 10^\circ\text{N}$. South of 10°N , in general, the continental influence starts decreasing and becomes almost insignificant near the equator ($0\text{--}5^\circ\text{N}$ region). This shows that on an average the intrusion of northern hemispheric continental air to the Southern Hemisphere is minimal except for the cross equatorial flow around $40\text{--}45^\circ\text{E}$ during February. On an average, an increasing trend in AOD is observable over the Arabian Sea and Bay of Bengal during 1996 to 1999, which later decreased and levelled off after 2002.

In general, the southern hemispheric Indian Ocean is relatively pristine except for some locations in certain periods of the year. In the eastern part of Indian Ocean this influence is observed during September to November. This impact remains more-or-less confined to north of 10°S and east of 70°E . In the western parts of the southern hemispheric Indian Ocean, south of 10°S , the continental influence is observable during the same period in the region west of 45°E . The continental influence is negligible in other parts of Indian Ocean, which is especially true south of 10°S . The influence of cross equatorial flow and inter-hemispheric transport is observed during February in the longitude region west of 45°E up to 15°S .

Acknowledgements

The Level 1b data of AVHRR used in this analysis was obtained from the NOAA Satellite Active Archive: <http://www.class.noaa.gov>. The operational products (AOD and Angstrom exponent) from MODIS used for comparison were obtained directly from the website: ftp://ladsftp.nascom.nasa.gov/allData/5/MOD08_M3/2002. The authors also acknowledge the NOAA Air Resources Laboratory (ARL) for the provision of the HYSPLIT transport and dispersion model and READY website: <http://www.arl.noaa.gov/ready.html>, used in this study.

References

- Blanchard D C and Woodcock A H 1957 Bubble formation and modification in the Sea and its meteorological significance; *Tellus* **9** 145–158.
- Cochrane M A 2003 Fire science for rainforests; *Nature* **421** 913–919.
- Cox C and Munk W 1954 Measurement of the roughness of the sea surface from photographs of the sun-glitter; *J. Opt. Soc. Am.* **44** 838–850.
- Draxler R R and Rolph G D 2003 HYSPLIT (HYbrid Single-Particle Lagrangian Integrated Trajectory) Model access via NOAA ARL READY Website (<http://www.arl.noaa.gov/ready/hysplit4.html>) NOAA Air Resources Laboratory, Silver Spring, MD.
- Erickson D J, Merrill J T and Duce R A 1986 Seasonal estimates of global atmospheric sea-salt distribution; *J. Geophys. Res.* **91** 1067–1072.
- Exton H J, Latham J, Park P M, Perry S J, Smith M H and Allan R R 1985 The production and dispersal of marine aerosol; *Q. J. Roy. Meteorol. Soc.* **111** 817–837.
- Fitzgerald J W 1991 Marine aerosols: A review; *Atmos. Environ.* **25A** 533–545.
- Gathman S G 1983 Optical properties of the marine aerosol as predicted by the navy aerosol model; *Opt. Eng.* **22** 57–62.
- Gong S L, Barrie L A and Blanchet J P 1997 Modeling of sea-salt aerosols in the atmosphere 1 Model development; *J. Geophys. Res.* **102** 3805–3818.
- Hoppel W A, Fitzgerald J W, Frick G M and Larson R E 1990 Aerosol size distribution and optical properties found in the marine boundary layer over the Atlantic Ocean; *J. Geophys. Res.* **95** 3659–3686.
- Husar H B, Prospero J M and Stowe L L 1997 Characterisation of tropospheric aerosols over the ocean with NOAA advanced very high-resolution radiometer optical thickness operational product; *J. Geophys. Res.* **102** 16,889–16,909.
- Jaenicke R 1984 Physical aspects of atmospheric aerosol in Aerosols and their climatic effects; (eds) H E Gerbard and A Deepak, A Deepak Publishing Hampton Virginia, pp 7–34.
- Jayaraman A, Lubin D, Ramachandran S, Ramanathan V, Woodbridge E, Collins D and Zalpuri K S 1998 Direct observations of aerosol radiative forcing over the tropical Indian Ocean during the January–February 1996 pre-INDOEX cruise; *J. Geophys. Res.* **103** 13,827–13,836.
- Jayaraman A, Satheesh S K, Mitra A P and Ramanathan V 2001 Latitude gradient in aerosol properties across the Inter Tropical Convergence Zone: results from the joint Indo-US study onboard Sagar Kanya; *Curr. Sci.* **80** 128–137.
- Kamra A K, Murugavel P, Pawar S D and Gopalakrishnan V 2001 Background aerosol concentration derived from the atmospheric electric conductivity measurements made over the Indian Ocean during INDOEX; *J. Geophys. Res.* **106** 28,643–28,651.
- Leck C, Larsson U, Bagander L E, Jojansson S and Hajdu S 1990 Di-methyl sulphide in the Baltic Sea: annual variability in relation to biological activity; *J. Geophys. Res.* **95** 3353–3363.
- Lovett R F 1978 Quantitative measurement of airborne sea-salt in the North Atlantic; *Tellus* **30** 358–364.
- Levine J S 1999 The 1997 fires in Kalimantan and Sumatra, Indonesia: Gaseous and particulate emissions, *Geophys. Res. Lett.* **26** 815–818.
- Monahan E C, Davidson K L and Spiel D E 1982 White cap aerosol productivity deduced from simulation tank measurements; *J. Geophys. Res.* **87** 8898–8904.
- Monahan E C 1971 Onset of white capping; *J. Phys. Oceanogr.* **1** 139–144.
- Moorthy K K, Satheesh S K and Murthy B V K 1997 Investigations of marine aerosols over the tropical Indian Ocean; *J. Geophys. Res.* **102** 18827–18842.
- Moorthy K K, Satheesh S K and Murthy B V K 1998 Characteristics of spectral optical depths and size distributions of aerosols over tropical oceanic regions; *J. Atmos. Solar Terr. Phys.* **60** 981–992.
- Moorthy K K, Niranjana K, Narasimhamurthy B, Agashe V V and Murthy B V K 1999 Aerosol climatology over India 1 ISRO GBP MWR Network and database: Scientific Report ISRO GBP SR 03 99, Indian Space Research Organization India.

- Moorthy K K and Satheesh S K 2000 Characteristics of aerosols over a remote island Minicoy in Arabian Sea: Optical properties and retrieved size characteristics; *Q. J. Roy. Meteorol. Soc.* **126** 81–109.
- Moorthy K K and Satheesh S K 2001 Aerosol characteristics over Minicoy: Evidence of influence of mineral dust transport; *J. Mar. Atmos. Res.* **2** 26–32.
- Moorthy K K, Saha A, Prasad B S N, Niranjana K, Jhurry D and Pillai P S 2001 Aerosol optical depth over peninsular India and adjoining oceans during the INDOEX campaigns: spatial, temporal, and spectral characteristics; *J. Geophys. Res.* **106** 28,539–28,554.
- Moorthy K K, Babu S S and Satheesh S K 2005 Aerosol characteristics and radiative impacts over the Arabian Sea during the intermonsoon season: Results from ARMEX field campaign; *J. Atmos. Sci.* **62** 192–206.
- Moorthy K K and Babu S S 2006 Aerosol back carbon over Bay of Bengal observed from an Island location, Port Blair: temporal features and long-range transport *J. Geophys. Res.* **111** D17205, doi:10.1029/2005JD006855.
- Nair S K, Rajeev K and Parameswaran K 2003 Winter time regional aerosol distribution and the influence of continental transport over the Indian Ocean; *J. Atmos. Sol. Terr. Phys.* **65** 149–165.
- Nair S K, Rajeev K and Parameswaran K 2004 Cloud screening in IRS-P4 OCM satellite data: potential of spatial coherence method in the absence of thermal channel information; *Remote Sensing Env.* **90** 259–267.
- Nair S K, Parameswaran K and Rajeev K 2005 Seven-year satellite observations of the mean structure and variabilities in the regional distribution of the oceanic areas around the Indian subcontinent; *Ann. Geophys.* **23** 1–20.
- Page S E, Siegert F, Rieley J O, Beohm H D V, Jaya A and Limin S 2002 The amount of carbon released from peat and forest fires in Indonesia during 1997; *Nature* **420** 61–65.
- Parameswaran K, Vijayakumar G, Murthy B V K and Moorthy K K 1995 Effect of wind speed on mixing region aerosol concentrations in a tropical coastal environment; *J. Appl. Meteorol.* **34** 1392–1397.
- Parameswaran K, Rajan R, Vijayakumar G, Rajeev K, Moorthy K K, Nair P R and Satheesh S K 1998 Seasonal and long term variations of aerosol content in the atmospheric mixing region at a tropical station on the Arabian Sea coast; *J. Atmos. Sol. Terr. Phys.* **60** 17–25.
- Parameswaran K, Nair S K and Rajeev K 2004 Impact of Indonesian forest fires during the 1997 El Niño on the aerosol distribution over the Indian Ocean; *Adv. Space. Res.* **33** 1098–1103.
- Prabha R Nair, Parameswaran K, Sunil Kumar S V and Rajan R 2004 Continental influence on the spatial distribution of particulate loading over the Indian Ocean during winter season; *J. Atmos. Sol. Terr. Phys.* **66** 27–38.
- Prabha R Nair, Parameswaran K, Annamma A and Salu J 2005 Wind dependence of sea-salt and non-sea-salt aerosols over the oceanic environment; *J. Atmos. Sol. Terr. Phys.* **67** 844–898 doi:10.1016/j.jastp.2005.02.008.
- Rajeev K, Ramanathan V and Meywerk J 2000 Regional aerosol distribution and its long-range transport over the Indian Ocean; *J. Geophys. Res.* **105** 2029–2043.
- Rajeev K and Ramanathan V 2001 Direct observations of clear-sky aerosol radiative forcing from space during the Indian Ocean Experiment; *J. Geophys. Res.* **106** 17,221–17,236.
- Ramachandran S 2004 Spectral aerosol optical characteristics during the northeast monsoon over the Arabian Sea and tropical Indian Ocean: 1. Aerosol optical depths and their variabilities; *J. Geophys. Res.* **109** D19207, doi:10.1029/2003JD004476.
- Ramachandran S 2005 Aerosol radiative forcing over Bay of Bengal and Chennai: Comparison with maritime, continental, and urban aerosol models; *J. Geophys. Res.* **110** D21206, doi:10.1029/2005JD005861.
- Ramanathan V, Crutzen P J, Lelieveld J, Mitra A P, Althausen D, Anderson J, Andreae M O, Cantrell W, Cass G R, Chung C E, Clarke A D, Coakley J A, Collins W D, Conant W C, Dulac F, Heintzenberg J, Heymsfield A J, Holben B, Howell S, Hudson J, Jayaraman A, Kiehl J T, Krishnamurti T N, Lubin D, McFarquhar G, Novakov T, Ogren J A, Podgorny I A, Prather K, Priestley K, Prospero J M, Quinn P K, Rajeev K, Rasch P, Rupert S, Sadourny R, Satheesh S K, Shaw G E, Sheridan P and Valero F P J 2001 Indian Ocean Experiment: An integrated analysis of the climate forcing and effects of the great Indo-Asian haze; *J. Geophys. Res.* **106** 28,371–28,398.
- Rolph G D 2003 Real-time Environmental Applications and Display System (READY) Website (<http://www.arl.noaa.gov/ready/hysplit4.html>) NOAA Air Resources Laboratory, Silver Spring, MD.
- Satheesh S K and Moorthy K K 1997 Aerosol characteristics over coastal regions of the Arabian Sea; *Tellus* **49B** 417–428.
- Satheesh S K, Moorthy K K and Murthy B V K 1998 Special gradients in aerosol characteristics over the Arabian Sea and Indian Ocean; *J. Geophys. Res.* **103** 26,183–26,192.
- Satheesh S K, Moorthy K K and Indrani Das 2001 Aerosol spectral optical depths over the Bay of Bengal, Arabian Sea and Indian Ocean; *Curr. Sci.* **81** 1617–1625.
- Satheesh S K, Ramanathan V, Holben B N, Moorthy K K, Loeb N G, Maring H, Prospero J M and Savoie D 2002 Physical chemical and radiative properties of Indian Ocean aerosols; *J. Geophys. Res.* **107** 10 1029/2002JD002463.
- Smith M H, Consterdine I E and Park P M 1989 Atmospheric loading of marine aerosols during a Hebridean cyclone; *Q. J. Roy. Meteorol. Soc.* **115** 383–395.
- Smith M H, Park P M and Consterdine I E 1993 Marine aerosols concentrations and estimated flux over the sea; *Q. J. Roy. Meteorol. Soc.* **119** 809–820.
- Turner S M, Malin G, Liss P S, Harbour D S and Holligan P M 1988 The seasonal variation of Di-methyl sulphoniopropionate concentrations in near shore waters; *Limnol. Oceanograph.* **33** 364–375.
- Vinoj V and Satheesh S K 2003 Measurements of aerosol optical depth over Arabian Sea during summer monsoon season; *Geophys. Res. Lett.* **30** doi:10.1029/2002GL016664.
- Woodcock A H 1953 Salt nuclei in marine air as a function of altitude and wind force; *J. Meteorol.* **10** 362–371.
- Wu J 1993 Production of spume drops by wind tearing of wave crests: The search for quantification; *J. Geophys. Res.* **98** 18,221–18,227.
- Zhang J, Reid J S and Holben B N 2005 An analysis of potential cloud artefacts in MODIS over ocean aerosol optical thickness products; *Geophys. Res. Lett.* **32** L15803 doi:10.1029/2005GL023254.